Photoacoustics 13 (2019) 25–32

Contents lists available at ScienceDirect

Photoacoustics

journal homepage: www.elsevier.com/locate/pacs

Research article

Raster-scan optoacoustic angiography of blood vessel development in colon cancer models

Anna Orlova[a,*], Marina Sirotkina[b], Ekaterina Smolina[a], Vadim Elagin[b], Andrey Kovalchuk[a], Ilya Turchin[a], Pavel Subochev[a]

[a] Institute of Applied Physics, Russian Academy of Sciences, 46 Ulyanov Str., Nizhny Novgorod 603950, Russia
[b] Privolzhsky Medical Research University, 10/1 Minin & Pozharsky sq., Nizhny Novgorod 603950, Russia

ARTICLE INFO

Keywords:
Optoacoustic imaging
Colon cancer models
Tumor vessel development

ABSTRACT

Raster-scan optoacoustic angiography at 532 nm wavelength with 50 μm lateral resolution at 2 mm diagnostic depth was used for quantitative characterization of neoangiogenesis in colon cancer models. Two tumor models of human colon adenocarcinoma (HT-29) and murine colon carcinoma (CT26) different in their histology and vascularization were compared. Tumors of both origins showed an inhomogeneous distribution of areas with high and low vascularization. Rapidly growing CT26 tumor demonstrated a higher rate of vessel growth from the periphery to the center. Peculiarities of the vascularity of tumor models revealed by optoacoustic imaging were confirmed by fluorescent microscopy with FITC-dextran and morphological analysis. The obtained results may be important for the investigation of tumor development and for improvement of colon cancer treatment strategies.

1. Introduction

Neoangiogenesis is one of the most important factors of cancer progression and metastases formation. Rapidly growing tumor mass with rising requirements in oxygen and nutrients stimulates vascular growth by producing various angiogenic factors [1]. With the growth of newly vascularized areas of the tumor, cancer cells cease to receive enough oxygen from the blood flow and form hypoxic regions. Hypoxia stimulates angiogenesis, that leads to further tumor growth, which in turn requires formation of new blood vessels. The angiogenic trigger thus remains switched on and new vessels continue to grow, increasing the blood supply and heterogeneity of the tumor. Continuous releasing of angiogenic factors limits the possibility of adequate development of mature vessels [2], leading to structural and physiological vascular abnormalities. Tortuosity, intricate loops, arteriovenous shunts, absence of well-defined systematization are the main features of tumor vessels that disrupt blood flow. A non-integral or damaged endothelial layer and a discontinuous basal membrane promote the increased vascular permeability, which dramatically increases the tumor interstitial pressure [3,4]. All these factors determine a hypoxic microenvironment, limitations of drug delivery to tumor cells and loss of sensitivity to treatment.

Degrees of vascularity vary in different types of malignant tumors as well as within one type of tumor. For tumors of some localizations, microvessel density was suggested to be a significant prognostic indicator [5]. Characteristic features of angiogenesis intensity and vessel maturation have been established for a series of neoplasms [6], a positive correlation between the expression of angiogenic factors and prognosis has been described [7]. There is an assumption that the effectiveness of therapy, at least of antiangiogenic therapy, is determined by the peculiarities of tumor vascularization [6].

Colon cancer is the most common gastrointestinal tumor. For most patients with metastatic colon cancer, palliative chemotherapy is the only present option; therefore, improved outcomes through new therapeutic strategies are desperately needed. Colon cancer is shown to be among the most angiogenic types of tumors [6]. Increased vascularity in this type of tumor in comparison with adenomas and normal tissues as well as with low-grade and high-grade dysplasia has been demonstrated in clinical studies [8,9]. It also had been shown that distant metastases formation is in good correlation with microvessel density [10]. Angiogenic factors that regulate the angiogenesis in human and murine colorectal tumors are identified and correlation of their expression level with prognosis has been proven [11].

It is reasonable to assume that the choice of treatment conditions, especially in the cases of anti-angiogenic and anti-vascular therapy, should be carried out individually for each tumor type or even for each

* Corresponding author.
E-mail address: orlova@ufp.appl.sci-nnov.ru (A. Orlova).

https://doi.org/10.1016/j.pacs.2018.11.005
Received 19 July 2018; Received in revised form 19 October 2018; Accepted 13 November 2018
Available online 23 November 2018

tumor. The involvement of new angiographic approaches in clinical practice will enable selection of tumors for particular types of treatment, thereby facilitating individualization of therapy. Moreover, understanding the features of the circulatory bed of malignant neoplasms may contribute to the development of new diagnostic approaches, as well as the procedures of assessment of tumor response to treatment.

Currently the gold standard of diagnostics of tumor vascularization is immunohistochemical counting of microvascular density *ex vivo* using specific endothelial markers [5]. Immunohistochemical analysis makes it possible to study the vascular pattern of a certain number of tissue samples, but it is limited in assessment of distribution of highly and low vascularized areas within the entire tumor volume, which is commonly uneven. In addition, as with any morphological approach, this method is unsuitable for monitoring studies. That is why a number of methods for non-invasive *in vivo* determination of particular morphological and functional parameters of the tumor vascular bed are being developed and tested in experimental and clinical oncology. The most progressive methods [12–14], such as computed tomographic angiography, magnetic resonance imaging and positron emission tomography require the injection of contrast agents or utilization of ionizing radiation. Safe and cost-effective methods of Doppler ultrasonography suffer from low contrast. Optical methods of optical coherence tomography angiography (OCTA) and fluorescence microscopic [12–14] and macroscopic [15] imaging are being actively developed. Nevertheless, OCTA and fluorescence microscopy are limited by diagnostic depth, and fluorescence macroscopic techniques are limited by spatial resolution [16]. While OCTA is label-free, it suffers from motion artifacts [17].

Hybrid methods of optoacoustic (OA) imaging [18,19] enable label-free angiography with optical contrast at optical penetration depths with ultrasonic resolution. Optoacoustic imaging is based on wideband registration of ultrasonic waves generated due to the absorption of pulsed laser radiation by optical chromophores. High OA contrast of the blood vessels is provided by high optical absorption of hemoglobin in red blood cells. Also various contrast agents can be used to enhance the visibility of internal structures [20,21] or in combination with treatment, to realize the theranostic approach [22–24]. Current promising applications of OA angiography include superficial tumor diagnostics in clinical oncology [25–27] and studies of tumor vascular pattern during growth and after the treatment of preclinical tumor models in experimental oncology [20,22,28–32].

Imaging of tumor vasculature has been done previously by different optoacoustic techniques. While optical-resolution photoacoustic microscopy [33] allowed an improved spatial resolution and limited diagnostic depth, tomographic approaches [20,34] allowed an improved diagnostic depth and limited spatial resolution.

Our system for raster-scan optoacoustic angiography [35] is based on dark-field optical illumination [28] and wide bandwidth ultrasonic detection [36] allowing to visualize individual blood vessels at up to 2.1 mm depths. The suggested approach [35] was used in this work for the first time for monitoring of tumor growth and quantitative characterization of tumor vascularity. We investigated the dynamics of blood vessel growth in experimental colon tumors. Two tumor models of human colon adenocarcinoma (HT-29) and murine colon carcinoma (CT26) were compared. These two models differ in their histology and vascularization and often used to test new antitumor therapies.

2. Materials and methods

2.1. Animals and tumor models

The experiments were carried out on 8-week-old female Nu/nu mice weighing 20–25 g. The animals were obtained from the “Pushchino” Nursery for laboratory animals (Moscow, Russia). The study was performed on two experimental colon cancer models: human adenocarcinoma HT-29 (ATCC No HTB-38) and murine carcinoma CT26 (ATCC No CRL-2638). Cells were injected intradermally into the outer side of both thighs (two tumor nodes per mouse) by standard protocol: HT-29 2×10^6 cells per 100 µl of PBS and CT26 2×10^5 cells per 100 µl PBS. The total number of tumors were 4 for HT-29 and 6 for CT26.

All experiments were performed in accordance with the European Convention for the Protection of Vertebrate Animals used for Experimental and Other Scientific Purposes (ETS 123) and The Guide for the Care and Use of Laboratory Animals, 8th edition (NRC 2011, National Academic Press).

2.2. OA imaging system and data processing

Raster-scan optoacoustic angiography was performed using the previously developed system [35,37]. A lateral/axial OA resolution of 50 µm/35 µm was provided by a focal spot of 35 MHz polyvinylidene fluoride detector with a 30 MHz bandwidth, $F = 6.8$ mm focal distance, and 0.6 numerical aperture. The sensitivity of our system allowed to visualize 50 µm blood vessels at up to 2.1 mm depth. Minimally detected diameter of blood vessel located at the surface of a soft tissue was 15 µm. However, if the size of blood vessel was less than 50 µm (system resolution), it was visualized as 50 µm blood vessel.

The scanning OA head was mounted on two computer-driven M-664 stages performing fixed lateral steps ($\delta x = \delta y = 25$ µm) within lateral scanning areas ($\Delta X = \Delta Y = 7.5$ mm) corresponding to the expected tumor size on the 13th day of growth. Computer-driven M-664 stages were mounted to a manual Z stage, which was used to provide OA focus at $Z = 1$ mm depth from the tissue surface. The low-jitter input of the laser Wedge HB 532 (BrightSolutions, Italy) was triggered by the scanning stages and provided optical pulses at a wavelength of 532 nm (isosbestic point for hemoglobin) with 1.4 ns duration and 1 mJ energy. The average radiant exposure at the tumor surface was 5 mJ/cm^2 complying with the ANSI Z136.1 standard for laser safety. OA A-scans corresponding to discrete XY positions of the scanning head were recorded by the first channel of two-channel 16-bit analog-to-digital converter (ADC) CSE1622 (Gage, USA) with 200 MS/s corresponding to $\Delta z \sim 7.6$ µm spatial sampling period in axial direction. The second channel of CSE1622 was used to collect the beam-sampling signal from a photodiode Det10a (Thorlabs, USA) equipped with a custom-made built-in integration circuit expanding the effective pulse duration to ~50 ns for better compatibility with the 200MS/s acquisition rate of the ADC.

After the acquisition of OA data, two post-acquisition algorithms were used to improve the resulting OA angiography images. At first, an acoustic reconstruction algorithm [38] was consequently applied to all XZ and YZ B-scans. After the reconstruction, XYZ OA data was reduced for every tumor according to the lateral (XY) size of each tumor on the 13th day and $Z = 2.1$ mm depth range ($Z = 0$ mm corresponded to the animal surface closest to the detector). Then, reconstructed XYZ OA data sets were processed by the Frangi filter [39] enhancing the contrast of vessel-like structures against ball-like or plate-like structures in 3D volume. For 2D representation of the vasculature, maximum intensity projections (MIP) to XY plane with color-encoded depth were calculated using the resulting 3D data sets. For quantitative characterization of the vasculature, grayscale MIP angiograms were used.

Obtained 2D angiographic images were then binarized using Fiji plug-in for ImageJ (NIH, USA) and the values of vascular density (percent of relationship between the square of vessels and the common tumor square) were calculated. The tumor zone was selected at the outer boundary of the peripheral small vessel area. Values for normal tissues were obtained at the beginning of the monitoring (5th day of tumor growth), when the tumor thickness did not exceed diagnostic depth (2.1 mm).

2.3. Animal study protocol

OA imaging was performed every 1–2 days for 9 days starting from

the 5th day after tumor inoculation. For OA study, the animals were anesthetized with Zoletil 100 (Virbac, France) and Rometar 2% (Bioveta, Czech Republic) injected intramuscularly, fixed on a support plate in a side position, the center of the tumor was aligned with the center of the scanning area.

Before each scanning, the tumor size was measured with a caliper in two mutually perpendicular directions. The tumor volumes were calculated by the formula $a \times b \times b/2$, where a is the measured length and b is the width of the tumor.

2.4. Fluorescent microscopy with FITC

On the 13th day of tumor growth OA data were verified by fluorescent microscopy (stereomicroscope Axio Zoom.V16, Zeiss, Germany) using Fluorescein isothiocyanate (FITC) conjugated with dextran 2MD (Sigma, USA). The ratio of FITC:glucose was 1:160. FITC was injected intravenously in the dose of 50 mg/kg of body weight. For excitation of fluorescence and emission detection, the following set of filters was used: excitation 470/40 nm, dichroic mirror 495 nm, emission 520/50 nm. The images were obtained within 10 min after FITC injection.

2.5. Morphological study

Verification of CT26 and HT-29 vascularization was carried out by histological examination on 13th day after tumor cells transplantation. The excised tumors were embedded in paraffin. Several cross sections (n = 3–5) were made from the tumor center. Histological preparations were stained with hematoxylin and eosin. Sections of 7 μm thickness were examined with light microscopy using Leica DM1000 system. Histopathology examination included evaluation of the percentage of tumor vessels in both tumor models.

2.6. Statistical analysis

For tumor volumes and vascular densities, the average values and standard deviation were calculated. The *t*-test for dependent samples was performed to determine the statistical significance of the difference between the values obtained at different time points from the baseline. The *t*-test for independent samples was employed for values obtained from two different tumor models. The threshold of statistical significance was taken at $p < 0.05$.

3. Results

Fig. 1 shows the examples of OA images of microvascular organization of HT-29 and CT26 colon tumor models at different time points of growth. OA images demonstrate the spatial distribution of individual blood vessels located at different depths of the tumor and normal tissues. Fig. 2 along with supplementary videos (S1, S2) visualize 3D vasculature of tumor and normal tissues at the depths of up to 2.1 mm.

Fig. 3a shows the dynamics of experimental tumor growth from the 5th to the 13th day after tumor inoculation, Fig. 3b – the average values of vascular density estimated by OA. During the monitoring period the HT-29 tumor volume increased up to 3 times from 81.5 ± 60.1 mm^3 to 224.5 ± 130.7 mm^3. Statistically significant changes compared to the baseline ($p < 0.05$) occurred on the 9th day after the injection of tumor cells. During the same period the CT26 tumor grew from 0.59 ± 0.84 mm^3 to 310.5 ± 8517 mm^3. For the CT26 model, statistically significant changes compared to the initial level were revealed from the 6th day after tumor inoculation. The dynamics of tumor growth varied at different periods of the tumor growths. Initially, on days 5th-7th, the mean volume of HT-29 was significantly higher than CT26 tumor volume ($p < 0.05$). Subsequently, starting from the 9th day tumor volumes of both CT26 and HT-29 became comparable, which was facilitated by the rapid growth of CT26. The obtained dynamics of tumor growth are in accordance with the data reported in [40,41] for HT-29 and CT26-bearing Nude mice.

Tumor growth was accompanied by the increase of their vascularity. At the beginning of monitoring, the bloodstream had already begun its formation and the vascular density in both tumor models was no less than 20% (Fig. 3b). From the 5th to the 7th day of tumor development, a gradual slow increase in the density of the vessels was demonstrated for the HT-29 model (upper row Fig. 1, Fig. 3b), statistically significant changes compared to the baseline ($p < 0.05$) occurred from day 7. At the same time the vascular density of CT26 model was not changing (lower row Fig. 1, Fig. 3b). As a result, on the 7th day of growth, a significant difference in the density of the vessels between HT-29 and CT26 occurred ($p < 0.05$). From the 9th day of tumor growth, the development of vessels in CT26 nodes began to accelerate, reaching statistically significant differences with the baseline on day 13. Tumors HT-29, on the contrary, demonstrated inhibition of vascular growth. On the 13th day of growth the vascular density of CT26 became higher than for HT-29. During the whole monitoring period, the vascular density of the HT-29 model increased by 1.6 times and of the CT26 model by 2.2 times. The average vascular density value of normal tissue (skin and muscle) surrounding the experimental tumor on the 1 st day of monitoring was calculated to be 40 ± 10%.

Fig. 4 shows the results of comparison of OA angiography with fluorescence microscopy on the 13th day of HT-29 and CT26 tumor growth. Both methods demonstrate thin, heterogeneously distributed blood vessels for HT-29. In contrast, for CT26 the fluorescence microscopy demonstrates larger FITC-stained zones, which also confirms the higher vascularity of CT26 tumor model revealed by OA angiography.

According to histological analysis (Fig. 5) murine colon carcinoma CT26 was represented by 98% of tumor parenchyma and only 1–2% of stroma. The tumor tissue had a dense structure and consisted of polymorphic cells with a diameter varying between 10 and 20 μm and round or oval nuclei. The slightly basophilic cytoplasm formed a thin ring around the nucleus. The blood vessels were presented by a dense network of tumor vessel sinusoids (neovasculature) with a diameter of approximately 10–15 μm; tumor capillaries and arterioles (up to 50–70 μm) were also found in CT26 histological slides (Fig. 5a). In contrast, human colon adenocarcinoma HT-29 was characterized by a larger percentage of tumor stroma (up to 5%). A small number of tumor sinusoids with an average diameter of 17 μm were observed in the HT-29 (Fig. 5b). Tumor capillaries or other vessels were not found.

4. Discussion

Development of novel approaches to study neoangiogenesis is essential for a better understanding of the mechanisms of their growth and for the progression of methods of specific blood vessel-targeted therapy control. We used 3D label-free OA angiography to study the dynamics of experimental models of colon cancer vascularization in the course of their natural growth. We obtained data on vascular shape, amount and density, as well as the spatial distribution of zones with different vascularization. The maximum diameter of blood vessels observed at OA angiograms did not exceed 100 μm.

With the use of two methods of vessel visualization, OA angiography and fluorescent microscopy (Fig. 4), similar data on the shape, size, and location of the vessels in the tumors were obtained. As opposed to optoacoustic microscope, fluorescent microscope did not allow to differentiate axial position of the blood vessels and provided at least 2-fold smaller imaging depth. Nevertheless, proper comparison of shape and lateral position of superficially located blood vessels could be performed by fluorescent and optoacoustic microscopy.

Both the HT-29 and CT26 tumor models were characterized as zones with small, tortuous, randomly distributed blood vessels as compared to normal surrounding tissues (Fig. 1). At the beginning of monitoring the density of the vessels in the tumor was two times lower than in the surrounding tissue, reflecting the insufficient development of tumor vasculature in the early stages of growth. By the end of the experiment,

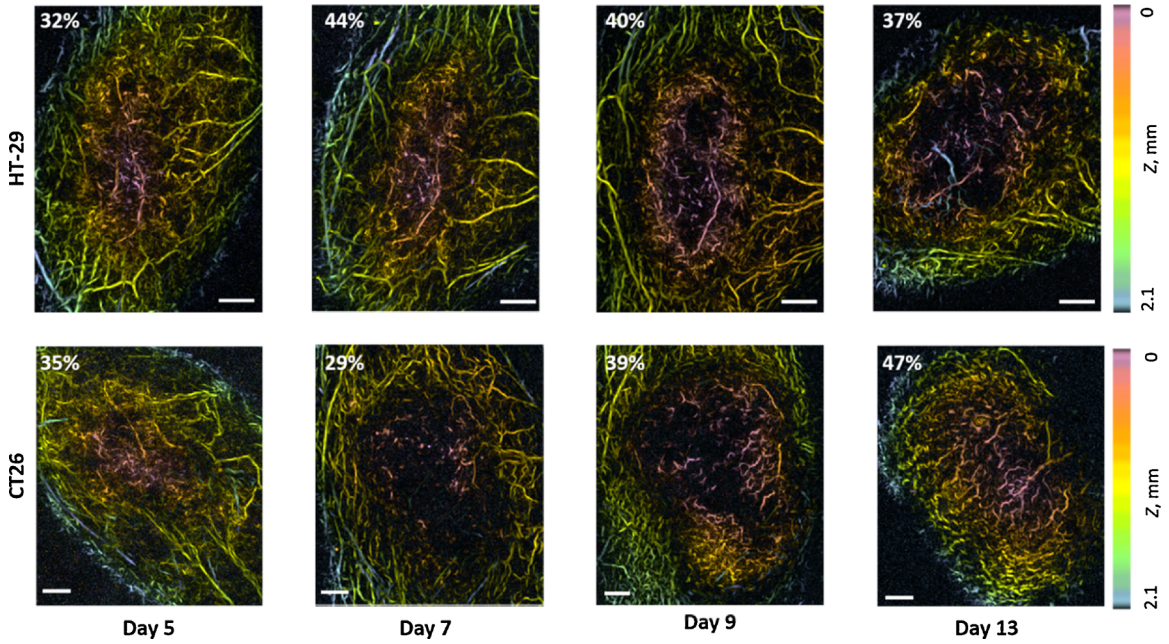

Fig. 1. OA-images of HT-29 and CT26 vasculature at different time points during tumor growth. The color scale encodes the depth of the corresponding blood vessels. Percent values characterize vascular density, $Z = 0$ mm corresponds to the animal surface, all bars are 1 mm.

the values of neoplastic and surrounding normal tissues became similar. OA angiography enabled differentiation between tumor and normal tissues based on vascular patterns and vascular densities.

Tumors of both origins showed an uneven distribution of areas with high and low vascularization, with a gradual decrease in vascular density from the periphery to the center. As the tumor grew, the vessels had progressively sprouted toward the center of the node. The observed type of vascular development is typical for the early stages of tumor growth [42], and a similar vascular pattern is demonstrated in various tumor models using different imaging techniques [33,43–45]. Another common feature of the investigated models is the heterogeneity of the vascular distribution from tumor to tumor within the group, which demonstrated by large standard deviations. In addition, for both models, the uneven vascular growth rate was shown during neoplasm development. There were stages of vessel growth deceleration; on some days of monitoring (7^{th}, 9^{th} days), due to faster growth of the tumor parenchyma the overall density of the vessels became smaller than on the previous day. Vascularization rate fluctuations were also noted for the CT26 tumor [44]. OA images revealed that the growth of blood vessels was slower than the growth of the tumor mass. At the same time, the largest area of avascular areas was observed on the days of tumor growth stimulation (9^{th}-13^{th} days for HT-29 and 7^{th}-9^{th} days for CT26).

Differences in the vascularization of the HT-29 and CT26 tumor models were manifested in the dynamics of their growth (Fig. 3b): in spite of the fact that the vascular density of HT-29 exceeded that of HT26 at the beginning of the experiment, CT26 showed a higher rate of vessel growth during the monitoring period and by the end of the experiment non-vascularized areas in this tumor were not observed. It can be assumed that the rapidly growing CT26 tumor (Fig. 3a) has greater requirements for oxygen and nutrients, intensive production of angiogenic factors, and, accordingly, a more active formation of blood vessels.

Fluorescence microscopy also demonstrated the higher vascularity of murine CT26 than human HT-29. Histological analysis revealed that the HT-29 model was poorly vascularized, demonstrating sinusoids of smaller diameter with slower perfusion. In contrast, CT26 had a rather developed microvascular network, and some large vessels were detected.

Data on the vascularity of HT-29 and CT26 had already been demonstrated using different *in vivo* and *ex vivo* methods. In the study [46], murine colon carcinoma CT26 was observed as well-vascularized by optical coherence angiography and fluorescent microscopy. In the study [47] CT26 was reported to be an optimal model for vascular-targeted photodynamic therapy because of its high vascular density detected by optical coherence angiography. The paper [48] was devoted to fluorescence assessment of HT-29 vascularization using AlexaFluor 750 conjugated with Bevacizumab. The study detected the VEGF expression in HT-29 colorectal cancer xenografts, signifying it as a potential agent for non-invasive imaging of VEGF expression. Also the strong staining by the anti-CD31 antibody was noted around the blood vessels, indicating a well-developed blood vessel network in HT-29. Burmakin et al [49] performed vascular analysis of HT-29 and CT26 tumor models by immunohistochemistry and showed that CT26 differed from HT-29 by higher vascularity.

It should be noted, that differences in size and position of the blood vessels could produce discrepancies in vascular density assessment. Although our OA system allowed to sense the blood vessels with diameter less than system resolution (50 μm), blood vessels of the smallest detectable size (15 μm) provided the same contribution to the vascular density as 50 μm ones. Therefore, our calculations of vascular density were more related to the number of vessels in the selected region, while rather insensitive to the vessel cross-section.

Although the sensitivity of our OA system allowed to detect 50 μm blood vessels through 0–2.1 mm depth range, due to the non-uniform distribution of optical fluence (challenged by curved surfaces of subcutaneous tumors) the maximum detectable depth of smaller vessels depended on the vessel's diameter. Small deeply located vessels producing too low optoacoustic signal could not contribute to MIP angiographic image and therefore shifted the vascular density to the lower value. Shifting of the vascular density to the lower value was also due to the limited numerical aperture of ultrasonic detector (as compared to full-view NA = 1 detector used in [50]), which did not allow to image vertical blood vessels (Fig. 2, supplementary videos S1, S2).

OA angiography enables visualization of the distribution of all hemoglobin-containing structures, but not their type and origin. Some tumors may be vascularized by angiogenesis or by using the pre-existing organ vasculature or by vascular mimicry [6]. For colon cancer,

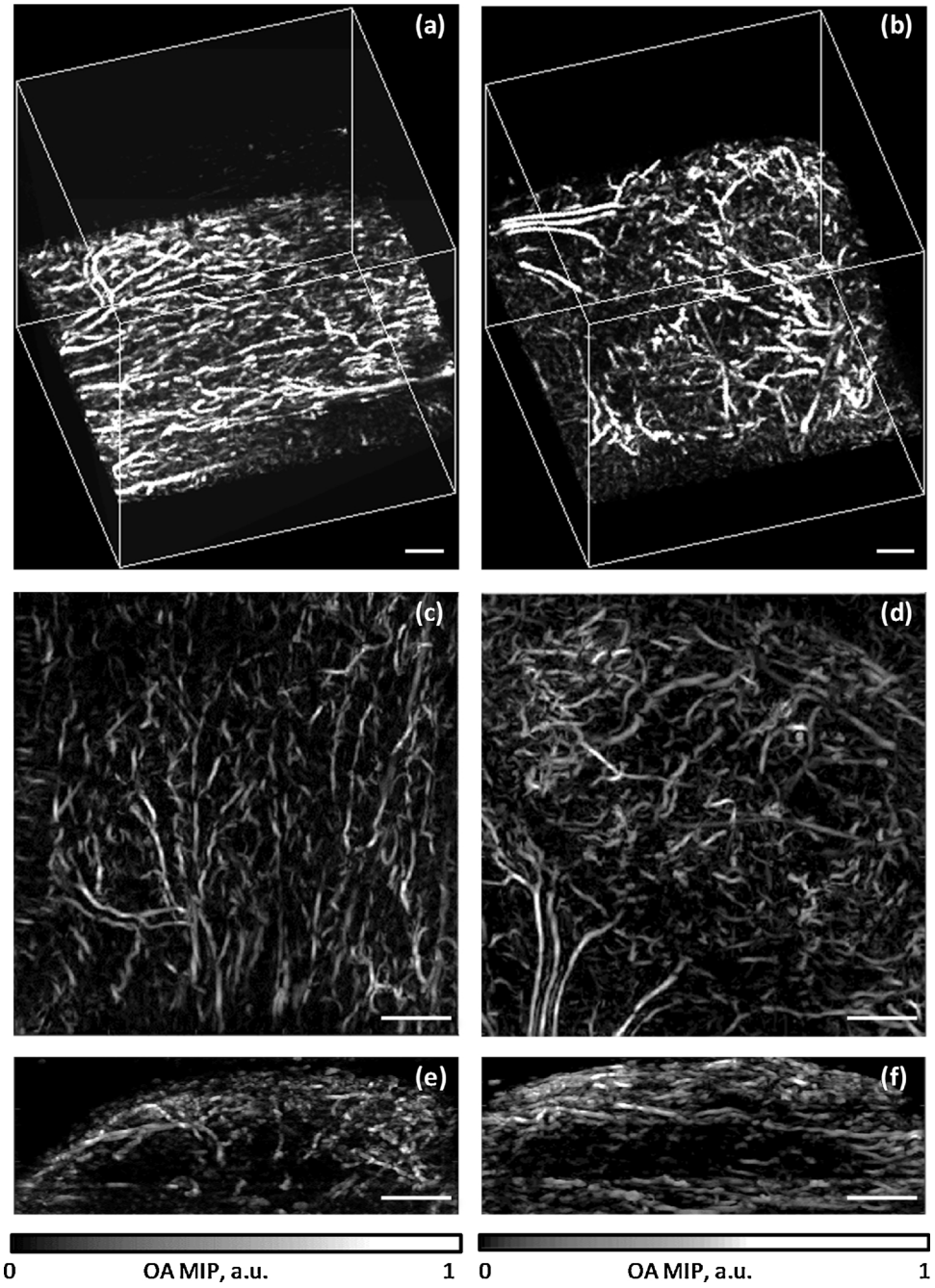

Fig. 2. Optoacoustic angiograms of normal tissue (left column) and HT-29 tumor on 13th day of growth (right column): (a,b) –visualization of 6x6x6 mm^3 vol; (c,d) – lateral MIPs; (e,f) – vertical MIPs. The presented 3D datasets can also be visualized in a movie files available in the on-line version of the journal (supplementary videos S1 and S2).

different types of blood vessels have been demonstrated [51,52]. Moreover, since 2.1 mm imaging depth was fixed for every tumor the projections of vasculature corresponding to normal tissue (skin and mussels) could increase the effective vascular density of smaller tumors at earlier stages of development. Nevertheless, OA angiography enabled differentiation between tumor or normal tissues, as well as capturing vessel distribution at different stages of tumor development. Such data may be significant for understanding the biological nature of the tumor microenvironment and for the improvement of cancer treatments.

5. Conclusions

We observed the dynamics of vascularization of two models of colon cancer using label-free raster-scan optoacoustic angiography. An increase in vascular density accompanying the tumor development was shown and the differences in vessel growth dynamics of two tumor models was demonstrated. Data on tumor vascularity obtained by OA were confirmed by the microscopy with fluorescent tracer FITC-dextran *in vivo* and by morphological study *ex vivo*. We demonstrated the possibilities of raster-scan angiography for the monitoring of neoangiogenesis and the quantitative comparison of vascularization between different tumor models. The developed approach is promising for assessment of the response of the tumor vascular system to different types of treatment.

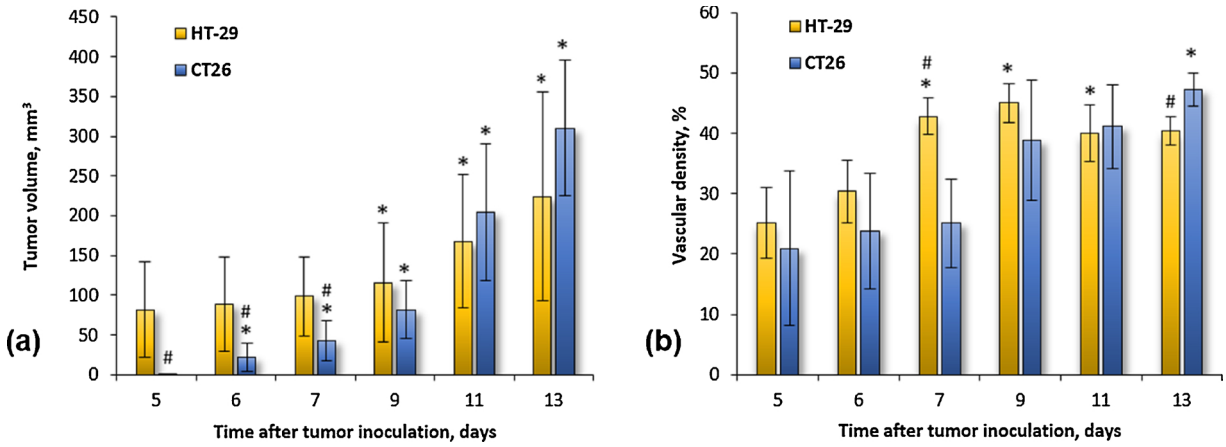

Fig. 3. Dynamics of HT-29 and CT26 tumors' growth (a) and vascular density (b). Asterisk (*) indicates statistically significant differences from the baseline on day 5 ($p < 0.05$). Hash (#) indicates statistically significant difference between current values for HT-29 and CT26 ($p < 0.05$).

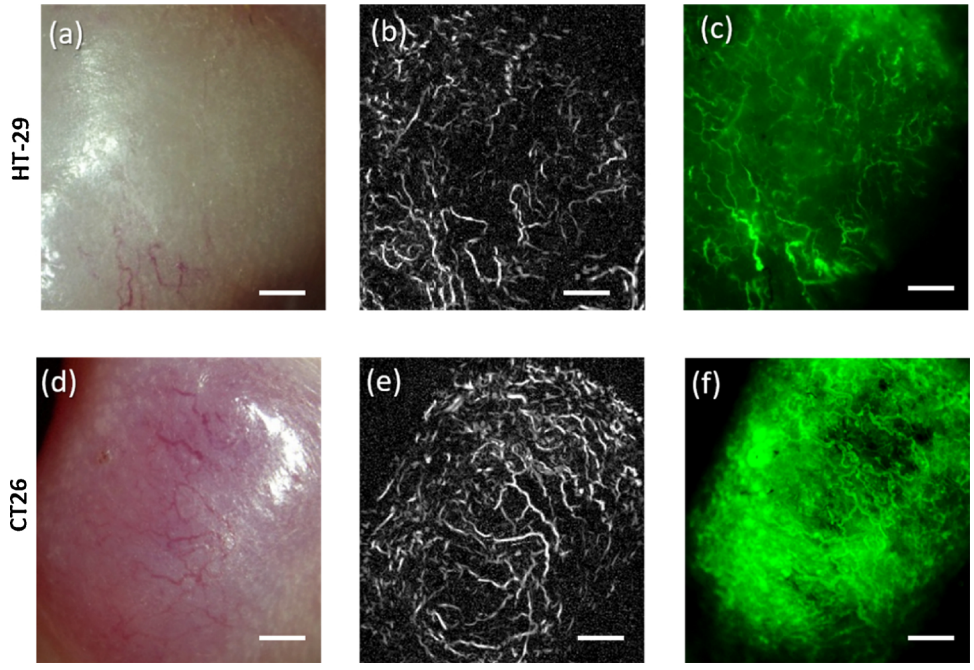

Fig. 4. Vessel structure of HT-29 (a–c) and CT26 (d–f) tumors on the 13th day of growth. (a, d) – photograph of tumor; (b, e) – maximum intensity projections obtained from OA data sets; (c, f) – fluorescence microscopy images. All bars are 1 mm.

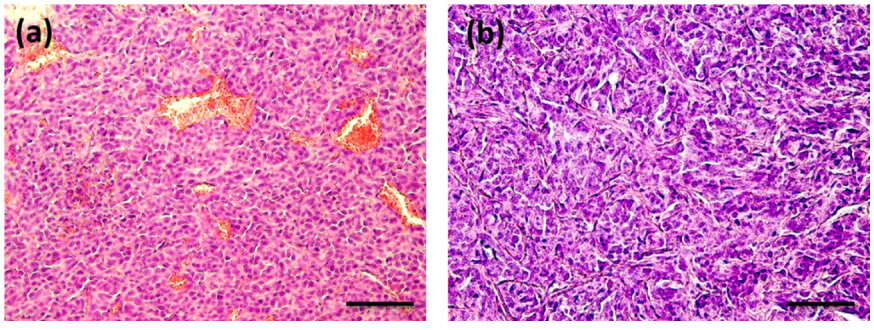

Fig. 5. Histological specimens of tumor tissues: (a) CT26 and (b) HT-29. Bar size 100 μm.

Conflict of interest

The authors declare there is no conflict of interest.

Funding

The work is supported by the Russian Science Foundation (project 14-15-00709-П).

Acknowledgments

The authors are grateful to Prof. Elena Zagaynova and Dr. Marina Shirmanova for their valuable contribution to the discussions; to Dr. Sergey Ksenofontov for providing software for 3D visualization; to Dr. Sergey Kuznetsov for tumor morphological analysis; to Dr. Michael Jaeger for provision of the reconstruction algorithm.

Appendix A. Supplementary data

Supplementary material related to this article can be found, in the online version, at doi:https://doi.org/10.1016/j.pacs.2018.11.005.

References

[1] S.M. Weis, D.A. Cheresh, Tumor angiogenesis: molecular pathways and therapeutic targets, Nat. Med. 17 (11) (2011) 1359.
[2] M. Plank, B. Sleeman, Tumour-induced angiogenesis: a review, J. Theor. Med. 5 (3-4) (2003) 137–153.
[3] J.M. Brown, W.R. Wilson, Exploiting tumour hypoxia in cancer treatment, Nat. Rev. Cancer 4 (6) (2004) 437.
[4] P. Vaupel, L. Harrison, Tumor hypoxia: causative factors, compensatory mechanisms, and cellular response, Oncologist 9 (Supplement 5) (2004) 4–9.
[5] B. Nico, V. Benagiano, D. Mangieri, N. Maruotti, A. Vacca, D. Ribatti, Evaluation of microvascular density in tumors: pro and contra, Histol. Histopathol. 23 (5) (2008) 601–607.
[6] A. Eberhard, S. Kahlert, V. Goede, B. Hemmerlein, K.H. Plate, H.G. Augustin, Heterogeneity of angiogenesis and blood vessel maturation in human tumors: implications for antiangiogenic tumor therapies, Cancer Res. 60 (5) (2000) 1388–1393.
[7] N. Nishida, H. Yano, T. Nishida, T. Kamura, M. Kojiro, Angiogenesis in cancer, Vasc. Health Risk Manage. 2 (3) (2006) 213.
[8] T. Cho, E. Shiozawa, F. Urushibara, N. Arai, T. Funaki, Y. Takehara, S. Tazawa, M. Misawa, M. Homma, T. Norose, The role of microvessel density, lymph node metastasis, and tumor size as prognostic factors of distant metastasis in colorectal cancer, Oncol. Lett. 13 (6) (2017) 4327–4333.
[9] K. Akagi, Y. Ikeda, Y. Sumiyoshi, Y. Kimura, J. Kinoshita, M. Miyazaki, T. Abe, Estimation of angiogenesis with anti-CD105 immunostaining in the process of colorectal cancer development, Surgery 131 (1) (2002) S109–S113.
[10] J.D. White, P.W. Hewett, D. Kosuge, T. McCulloch, B.C. Enholm, J. Carmichael, J.C. Murray, Vascular endothelial growth factor-D expression is an independent prognostic marker for survival in colorectal carcinoma, Cancer Res. 62 (6) (2002) 1669–1675.
[11] K. Rmali, M. Puntis, W. Jiang, Tumour-associated angiogenesis in human colorectal cancer, Colorectal Dis. 9 (1) (2007) 3–14.
[12] D.M. McDonald, P.L. Choyke, Imaging of angiogenesis: from microscope to clinic, Nat. Med. 9 (6) (2003) 713.
[13] A. Iagaru, S.S. Gambhir, Imaging tumor angiogenesis: the road to clinical utility, Am. J. Roentgenol. 201 (2) (2013) W183–W191.
[14] J. Ehling, T. Lammers, F. Kiessling, Non-invasive imaging for studying anti-angiogenic therapy effects, Thromb. Haemost. 109 (3) (2013).
[15] M. Yang, L. Li, P. Jiang, A. Moossa, S. Penman, R.M. Hoffman, Dual-color fluorescence imaging distinguishes tumor cells from induced host angiogenic vessels and stromal cells, Proc. Natl. Acad. Sci. 100 (24) (2003) 14259–14262.
[16] I.V. Turchin, Methods of biomedical optical imaging: from subcellular structures to tissues and organs, Physics-Uspekhi 59 (5) (2016) 487.
[17] D. Ferrara, Image artifacts in optical coherence tomography angiography, Clin. Exp. Ophthalmol. 44 (5) (2016) 367–368.
[18] L.V. Wang, S. Hu, Photoacoustic tomography: in vivo imaging from organelles to organs, Science 335 (6075) (2012) 1458–1462.
[19] X. Deán-Ben, S. Gottschalk, B. Mc Larney, S. Shoham, D. Razansky, Advanced optoacoustic methods for multiscale imaging of in vivo dynamics, Chem. Soc. Rev. 46 (8) (2017) 2158–2198.
[20] V. Ermolayev, X.L. Dean-Ben, S. Mandal, V. Ntziachristos, D. Razansky, Simultaneous visualization of tumour oxygenation, neovascularization and contrast agent perfusion by real-time three-dimensional optoacoustic tomography, Eur. Radiol. 26 (6) (2016) 1843–1851.
[21] W. Li, R. Chen, J. Lv, H. Wang, Y. Liu, Y. Peng, Z. Qian, G. Fu, L. Nie, In vivo photoacoustic imaging of brain injury and rehabilitation by high-efficient near-infrared dye labeled mesenchymal stem cells with enhanced brain barrier permeability, Adv. Sci. 5 (2) (2018) 1700277.
[22] Y. Cheng, X. Tan, J. Wang, Y. Wang, Y. Song, Q. You, Q. Sun, L. Liu, S. Wang, F. Tan, Polymer-based gadolinium oxide nanocomposites for FL/MR/PA imaging guided and photothermal/photodynamic combined anti-tumor therapy, J. Control. Release 277 (2018) 77–88.
[23] L. Nie, S. Wang, X. Wang, P. Rong, Y. Ma, G. Liu, P. Huang, G. Lu, X. Chen, In vivo volumetric photoacoustic molecular angiography and therapeutic monitoring with targeted plasmonic nanostars, Small 10 (8) (2014) 1585–1593.
[24] L. Nie, P. Huang, W. Li, X. Yan, A. Jin, Z. Wang, Y. Tang, S. Wang, X. Zhang, G. Niu, Early-stage imaging of nanocarrier-enhanced chemotherapy response in living subjects by scalable photoacoustic microscopy, ACS Nano 8 (12) (2014) 12141–12150.
[25] M. Toi, Y. Asao, Y. Matsumoto, H. Sekiguchi, A. Yoshikawa, M. Takada, M. Kataoka, T. Endo, N. Kawaguchi-Sakita, M. Kawashima, Visualization of tumor-related blood vessels in human breast by photoacoustic imaging system with a hemispherical detector array, Sci. Rep. 7 (2017) 41970.
[26] A.B.E. Attia, S.Y. Chuah, D. Razansky, C.J.H. Ho, P. Malempati, U. Dinish, R. Bi, C.Y. Fu, S.J. Ford, J.S.-S. Lee, Noninvasive real-time characterization of non-melanoma skin cancers with handheld optoacoustic probes, Photoacoustics 7 (2017) 20–26.
[27] H. Ma, S. Yang, Z. Cheng, D. Xing, Photoacoustic confocal dermoscope with a waterless coupling and impedance matching opto-sono probe, Opt. Lett. 42 (12) (2017) 2342–2345.
[28] H.F. Zhang, K. Maslov, G. Stoica, L.V. Wang, Functional photoacoustic microscopy for high-resolution and noninvasive in vivo imaging, Nat. Biotechnol. 24 (7) (2006) 848.
[29] V. Neuschmelting, K. Kim, J. Malekzadeh-Najafabadi, S. Jebiwott, J. Prakash, A. Scherz, J.A. Coleman, M.F. Kircher, V. Ntziachristos, WST11 Vascular targeted photodynamic therapy effect monitoring by multispectral optoacoustic tomography (MSOT) in Mice, Theranostics 8 (3) (2018) 723.
[30] L.J. Rich, M. Seshadri, Photoacoustic monitoring of tumor and normal tissue response to radiation, Sci. Rep. 6 (2016) 21237.
[31] I. Quiros-Gonzalez, M.R. Tomaszewski, S.J. Aitken, L. Ansel-Bollepalli, L.-A. McDuffus, M. Gill, L. Hacker, J. Brunker, S.E. Bohndiek, Optoacoustics delineates murine breast cancer models displaying angiogenesis and vascular mimicry, Br. J. Cancer 118 (8) (2018) 1098.
[32] S. Mallidi, K. Watanabe, D. Timerman, D. Schoenfeld, T. Hasan, Prediction of tumor recurrence and therapy monitoring using ultrasound-guided photoacoustic imaging, Theranostics 5 (3) (2015) 289.
[33] R. Lin, J. Chen, H. Wang, M. Yan, W. Zheng, L. Song, Longitudinal label-free optical-resolution photoacoustic microscopy of tumor angiogenesis in vivo, Quant. Imaging Med. Surg. 5 (1) (2015) 23.
[34] J.G. Laufer, E.Z. Zhang, B.E. Treeby, B.T. Cox, P.C. Beard, P. Johnson, B. Pedley, In vivo preclinical photoacoustic imaging of tumor vasculature development and therapy, J. Biomed. Opt. 17 (5) (2012) 056016.
[35] P. Subochev, Cost-effective imaging of optoacoustic pressure, ultrasonic scattering, and optical diffuse reflectance with improved resolution and speed, Opt. Lett. 41 (5) (2016) 1006–1009.
[36] M. Omar, M. Schwarz, D. Soliman, P. Symvoulidis, V. Ntziachristos, Pushing the optical imaging limits of cancer with multi-frequency-band raster-scan optoacoustic mesoscopy (RSOM), Neoplasia 17 (2) (2015) 208–214.
[37] P. Subochev, A. Orlova, I. Mikhailova, N. Shilyagina, I. Turchin, Simultaneous in vivo imaging of diffuse optical reflectance, optoacoustic pressure, and ultrasonic scattering, Biomed. Opt. Express 7 (10) (2016) 3951–3957.
[38] M. Jaeger, S. Schüpbach, A. Gertsch, M. Kitz, M. Frenz, Fourier reconstruction in optoacoustic imaging using truncated regularized inverse k-space interpolation, Inverse Probl. 23 (6) (2007) S51.
[39] T. Oruganti, J.G. Laufer, B.E. Treeby, Vessel filtering of photoacoustic images, Proc. SPIE, (2013), p. 85811W.
[40] S. Radulovic, G. Miller, A.V. Schally, Inhibition of growth of HT-29 human colon cancer xenografts in nude mice by treatment with bombesin/gastrin releasing peptide antagonist (RC-3095), Cancer Res. 51 (21) (1991) 6006–6009.
[41] P. Zhou, L. L'italien, D. Hodges, X.M. Schebye, Pivotal roles of CD4+ effector T cells in mediating agonistic anti-GITR mAb-induced-immune activation and tumor immunity in CT26 tumors, J. Immunol. 179 (11) (2007) 7365–7375.
[42] G.D. Yancopoulos, S. Davis, N.W. Gale, J.S. Rudge, S.J. Wiegand, J. Holash, Vascular-specific growth factors and blood vessel formation, Nature 407 (6801) (2000) 242.
[43] V. Demidov, A. Maeda, M. Sugita, V. Madge, S. Sadanand, C. Flueraru, I.A. Vitkin, Preclinical longitudinal imaging of tumor microvascular radiobiological response with functional optical coherence tomography, Sci. Rep. 8 (1) (2018) 38.
[44] J. Seguin, B.-T. Doan, H. Latorre Ossa, L. Jugé, J.-L. Gennisson, M. Tanter, D. Scherman, G.G. Chabot, N. Mignet, Evaluation of nonradiative clinical imaging techniques for the longitudinal assessment of tumour growth in murine CT26 colon carcinoma, Int. J. Mol. Imaging 2013 (2013).
[45] R.A. Byers, M. Fisher, N.J. Brown, G.M. Tozer, S.J. Matcher, Vascular patterning of subcutaneous mouse fibrosarcomas expressing individual VEGF isoforms can be differentiated using angiographic optical coherence tomography, Biomed. Opt. Express 8 (10) (2017) 4551–4567.
[46] M. Sirotkina, E. Kiseleva, E. Gubarkova, N. Buyanova, V. Elagin, V.Y. Zaitsev, L. Matveev, A. Matveev, M.Y. Kirillin, G. Gelikonov, Multimodal optical coherence tomography in the assessment of cancer treatment efficacy, Bull. Russ. State Med. Univ. 4 (2016).
[47] M. Sirotkina, L. Matveev, M. Shirmanova, V. Zaitsev, N. Buyanova, V. Elagin, G. Gelikonov, S. Kuznetsov, E. Kiseleva, A. Moiseev, Photodynamic therapy

monitoring with optical coherence angiography, Sci. Rep. 7 (2017) 41506.
[48] B. Paudyal, P. Paudyal, D. Shah, H. Tominaga, Y. Tsushima, K. Endo, Detection of vascular endothelial growth factor in colon cancer xenografts using bevacizumab based near infrared fluorophore conjugate, J. Biomed. Sci. 21 (1) (2014) 35.
[49] M. Burmakin, T. Wieringen, P.O. Olsson, L. Stuhr, A. Åhgren, C.-H. Heldin, R.K. Reed, K. Rubin, C. Hellberg, Imatinib increases oxygen delivery in extracellular matrix-rich but not in matrix-poor experimental carcinoma, J. Transl. Med. 15 (1) (2017) 47.
[50] X.L. Deán-Ben, H. López-Schier, D. Razansky, Optoacoustic micro-tomography at 100 volumes per second, Sci. Rep. 7 (1) (2017) 6850.
[51] C.I. Baeten, F. Hillen, P. Pauwels, A.P. de Bruine, C.G. Baeten, Prognostic role of vasculogenic mimicry in colorectal cancer, Dis. Colon Rectum 52 (12) (2009) 2028–2035.
[52] R. Bendardaf, A. Buhmeida, M. Hilska, M. Laato, S. SYRJÄNEN, K. SYRJÄNEN, Y. COLLAN, S. PYRHÖNEN, VEGF-1 expression in colorectal cancer is associated with disease localization, stage, and long-term disease-specific survival, Anticancer Res. 28 (6B) (2008) 3865–3870.

Anna Orlova (Ph.D.) is a senior scientist of the Laboratory of Biophotonics of the Institute of Applied Physics of RAS. She received her Ph.D. degree in biology in 2004 from Nizhny Novgorod State University. The major area of her research focuses on optical and optoacoustic imaging both in clinical and experimental oncology. Her main interests include investigation of tumor vascular microenvironment responses to treatments. Coauthor of more than 40 peer-review articles and several book chapters.

Marina Sirotkina (Ph.D.) is the Senior Researcher at the Institute of Biomedical Technologies, Privolzhsky Research Medical University. She graduated from the Biology Department of the Lobachevsky State University of Nizhny Novgorod, Russia in 2007 and received her Ph.D. in Biophysics in 2014. Since 2015 she is focused on optical bioimaging methods for angiography study, including optical coherence angiography and fluorescence bioimaging. Coauthor of 12 peer-review articles related to tumor angiography investigation.

Ekatrina Smolina (BS student) is a laboratory assistant at the Laboratory of Biophotonics of Institute of Applied Physics of Russian Academy of Sciences. Her current research focuses on the developing the methods of optoacoustic imaging of biological tissues.

Vadim Elagin is the Researcher at the Institute of Biomedical Technologies, Privolzhsky Research Medical University. He studied biophysics at the N.I. Lobachevsky State University of Nizhny Novgorod, Russia, where he received his Diploma in 2008. His scientific interests include cell culture studies, optical bioimaging, nonlinear microscopy and laser tissue interaction. Coauthor of 20 peer-review articles.

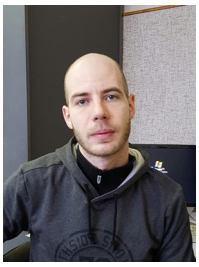

Andrey Kovalchuk (M.Sc., Ph.D. student) is a researcher at the Laboratory of Autowave-processes of Institute of Applied Physics of Russian Academy of Sciences. He received her Master degree in Physics in 2006 from Lobachevsky State University of Nizhni Novgorod. His current research focuses on the developing the methods of computational neural-networks and image processing.

Ilya Turchin (Ph.D.) is the Head of the Department for radiophysics methods in medicine at the Institute of Applied Physics of RAS and is an expert in optical imaging systems design (optical diffuse imaging, fluorescence imaging, photoacoustics) and biomedical applications. He has over 10 years of experience as a primary investigator in optical imaging, photodynamic therapy, and translation of optical techniques into clinics. He has published more than 50 peer-review articles.

Pavel Subochev (Ph.D.) is the optoacoustic group leader at the Laboratory of Biophotonics, Insitute of Applied Physics RAS. He graduated from Lobachevsky State University of Nizhni Novgorod in 2006 and received his PhD in passive acoustic radiometry from the Institute of Applied Physics of Russian Academy of Sciences. Since 2012 he is focused on the development of new instrumentation for optoacousutic imaging of biological tissues. Coauthor of 30 peer-review articles and conference proceedings related to optoacoustics.